

# PathGAN: Local Path Planning with Generative Adversarial Networks

Dooseop Choi, Seung-Jun Han, Kyoungwook Min, Jeongdan Choi  
 ETRI  
 Republic of Korea  
 d1024.choi@etri.re.kr

## Abstract

Targeting autonomous driving without High-Definition maps, we present a model capable of generating multiple plausible paths from sensory inputs for autonomous vehicles. Our generative model comprises two neural networks, Feature Extraction Network (FEN) and Path Generation Network (PGN). FEN extracts meaningful features from input scene images while PGN generates multiple paths from the features given a driving intention and speed. To make paths generated by PGN both be plausible and match the intention, we introduce a discrimination network and train it with PGN under generative adversarial networks (GANs) framework. Besides, to further increase the accuracy and diversity of the generated paths, we encourage PGN to capture intentions hidden in the positions in the paths and let the discriminator evaluate how realistic the sequential intentions are. Finally, we introduce ETRIDriving, the dataset for autonomous driving where the recorded sensory data is labeled with discrete high-level driving actions, and demonstrate the-state-of-the-art performances of the proposed model on ETRIDriving in terms of the accuracy and diversity.

## 1. Introduction

Autonomous driving has shown great advances in recent years owing to the breakthrough in sensor technology and artificial intelligence. Now a few companies are providing a commercial autonomous vehicle (AV) service in a limited area while others are testing their AVs with the goal of the commercial service. Most automated driving systems (ADSs) for AVs are known to rely on the algorithmic framework, which comprises three stages: *perception*, *planning*, and *control*, with the aid of High-Definition (HD) map. In *perception* stage, the system recognizes static and dynamic objects surrounding an AV in traffic scenes. Based on the recognition, it decides the next movements of the AV and controls the AV according to the decision in *planning* and *control* stages, respectively.

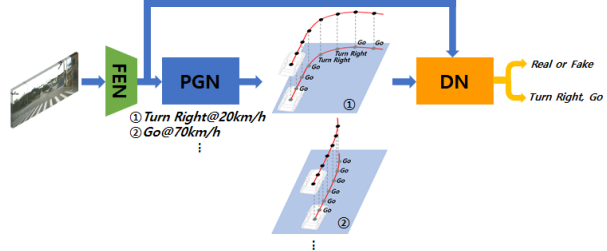


Figure 1. The brief description of *PathGAN*. Our path generation model is trained to generate multiple plausible paths from an egocentric view image given a driving intention and speed. Discrimination networks are simultaneously trained to encourage the generated paths to be plausible and match the intention.

HD map enables AVs to see beyond the coverage of the mounted sensors, providing an accurate representation of the road ahead and information on the surrounding environment [16]. In addition, the exact localization of AVs is ensured by the mapping of HD map data with surrounding lane lines or landmarks as reference positions. High dependence of AVs on HD map sometimes limits their ability to drive in diverse driving environments. For example, suppose a vehicle is on an unpaved road with traffic, human drivers can determine plausible paths for the vehicle by using contextual cues of the surroundings (e.g., shape of road, locations of static and dynamic objects), which can change over time. The conventional ADSs, however, may have trouble in determining the paths if HD map does not provide the cues for the area.

One of the solutions to this problem is to build a system that can extract the contextual cues from sensor outputs directly and use the cues for the control of the vehicles. Many approaches have been proposed in the literature to generate control signals (steering angle, speed) from sensory inputs [23, 6, 3, 31, 36, 8, 15, 34]. However, the existing methods have at least one of the following drawbacks: 1) they only generate control signals for one or a few maneuvers (*Go*, *Turn left/right*), 2) only one control signal is generated at a time, 3) the generated control signals are not

interpretable. Toward the ADS without HD map, we propose a model, which can generate multiple plausible paths from sensory inputs given a driving intention and speed. The paths generated by our proposed model are based on the ego-centric coordinate system, therefore, they are interpretable and can be used for the calculation of the control signals directly.

On the other hand, currently available autonomous driving datasets [28, 11, 9, 31, 15, 8] are not suitable for training path generation models with the aforementioned characteristics, since they provide only the recorded control signals with sensor outputs. Recently, Cai et al. [4] labeled every image in RobotCar dataset [21] with one of the three actions (*Go*, *Turn left/right*) for their trajectory prediction task. However, the three are not enough for defining the possible actions of the vehicle. In this paper, we classified possible actions of a vehicle into nine (*Go*, *Turn Left/Right*, *U-Turn*, *Left/Right Lane Change*, *Avoidance*, *Left/Right Way*) and manually assigned one of the nine actions to each frame of the recorded data, which we collected at 10Hz while driving in diverse driving conditions. We call our dataset *ETRIDriving* and will introduce it in the next section.

The main contributions of this paper are summarized as follows:

- We propose a generative model that can generate multiple plausible and interpretable paths from sensory inputs that match a driving intention and speed.
- We propose an interaction model between positions in a path and intentions hidden in the positions for improving the accuracy and diversity of the generated paths.
- We introduce *ETRIDriving*, the driving dataset labeled with the high-level driving actions.
- We evaluate our model on *ETRIDriving* and demonstrate the state-of-the-art performances in terms of the accuracy and diversity.

## 2. Related Works

**End-to-End Models** Approaches in this category train neural networks (NNs) to map sensory inputs to control signals such as steering angle and speed. The first attempt to exploit deep convolutional neural networks (CNNs) for the mapping was done by Bojarski et al. [3] where a CNN is trained to map a front-facing camera image to a steering angle. Motivated by [3], many end-to-end models have been proposed in the literature [31, 36, 8, 15, 34, 22, 17]. As mentioned in section 1, the models have drawbacks that they ignore either the multimodal nature of human driver’s action or the importance of the interpretability of the generated control signals. In general, human drivers consider multiple paths and drive along the one, which is selected by considering their driving intention and surroundings. However, the methods can’t provide multiple options at once. In

addition, the generated signals are not interpretable so that ADSs are not able to assess the risk of accepting the signals.

**Future Trajectory Forecasting** Trajectory forecasting has gained great attention in autonomous driving since predicting the future movements of the surrounding objects is essential for safe driving. In general, approaches in this category train recurrent neural networks (RNNs) to predict future trajectories of agents in a scene considering the scene context information available from sensory inputs [19, 1, 13, 26, 24, 25, 37, 7, 5, 27, 10]. Directly comparing our model with the models in this category may be inappropriate since ours aims at generating *paths* while the others predicting future *trajectories*. However, one may consider slightly modifying the existing models to generate paths instead of trajectories. From that point of view, our model shows several advantages over them as follows: 1) ours can generate multiple paths that match a driving intention, 2) prior distribution models, which needs to be trained in advance, are not required, 3) HD map is not required for the path generation. Recently, Cai et al. [4] proposed a model that estimates a future trajectory of the ego-vehicle from an egocentric view image and a driving intention. However, the model can deal with only three driving intentions (*Go*, *Turn left/right*). In addition, three different networks with the same structure need to be trained for the three driving intentions, respectively.

**Image Captioning** Image captioning is the process of generating textual descriptions of an image. Many approaches have been proposed in the literature [32, 30, 20, 35, 12, 33] and they generally follow the encoder-decoder architecture in which a CNN extracts features from an image while RNNs generate textual descriptions from the features. We design our path generation model inspired by the captioning models. Specifically, our approach has a close relationship with [12]. The authors of [12] proposed training their captioning model under GANs framework to make the model generate textual descriptions of diverse styles. Our approach is different from [12] in the following ways: 1) we design our model not only to generate *paths* that match a driving intention but also to find a hidden *intention* for each position in a path, 2) we propose an attentive discriminator, which takes as inputs the generated paths along with the visual features to evaluate if the paths are plausible and match a driving intention.

On the other hand, Aneja et al. [2] proposed capturing the intentions hidden in the generated words. Since they don’t have the ground-truth for the intentions, they trained their model to capture the intentions in a sequential latent space via Variational AutoEncoder. In contrast, we let our model directly learn the distribution of the sequential intentions for the positions via GANs framework. We also train our model to estimate the hidden intentions accurately at the same time, since *ETRIDriving* provides the ground-truth for

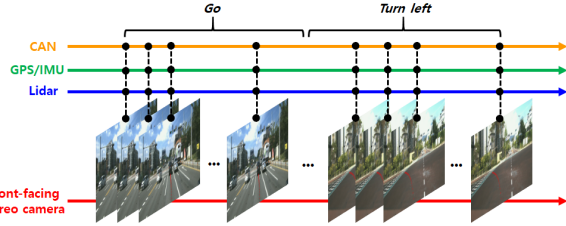


Figure 2. A brief description of our driving action labeling process.

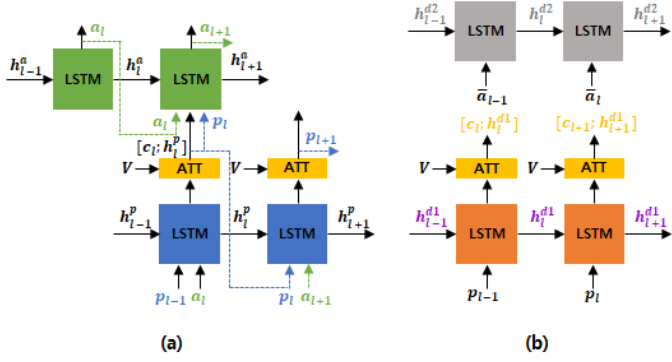


Figure 3. Brief descriptions of (a) path generation network and (b) discrimination network.

the intentions. Finally, we design our model to utilize the visual contexts effectively through an attention mechanism both for the path generation and intention decision.

### 3. ETRIDriving Dataset

We introduce *ETRIDriving*, the autonomous driving dataset labeled with the high-level driving actions of the ego-vehicle. To assemble *ETRIDriving*, we first collected data from the sensors (two front-facing cameras, GPS/IMU, CAN bus, and Lidar scanner) mounted on the vehicle (Genesis G80, Hyundai) while driving about 21 hours in various conditions and synchronized the data in time. Next, we assigned one of the nine actions to every frame in the data manually. For example, for the data collected while the ego-vehicle was turning left, we assigned *Turn left* label to the data. Figure 2 shows an example of the labeling process.

## 4. Proposed Model

### 4.1. Problem Definition

Let  $\mathbf{P}_a = [\mathbf{p}_1, \dots, \mathbf{p}_L]$  denote a path that matches a driving intention  $a$  determined by a planning system of an AV. Here  $\mathbf{p}_l \in \mathbf{R}^2$  is a position vector in an egocentric coordinate system centered on the AV and  $a$  is an element of driving action space  $\mathcal{A}$ . We define  $\mathcal{A}$  by using the nine actions described in section 1, consequently,  $a$  can be one of the nine actions. Also, let  $\mathbf{I}_t$  and  $s$  respectively denote raw data from sensors mounted on the AV at the current time  $t$

and the target speed of the AV. Then our target is to generate  $K$  plausible paths  $\{\mathbf{P}_a^k\}_{k=1}^K$  that match  $a$  from  $\mathbf{I}_t$  and  $s$ . In the rest of this paper, we omit the time index  $t$  for readability.

### 4.2. Model Architecture

The proposed path generation model consists of two networks, Feature Extraction Network (FEN) and Path Generation Network (PGN). FEN extracts meaningful features from sensory inputs while PGN produces paths from the features given the driving intention and the target speed. To make paths generated by PGN be plausible and match the intention, we introduce discrimination networks (DNs).

**FEN** In this paper, we use egocentric view images from a front-facing camera mounted on the AV as inputs to FEN. Consequently,  $\mathbf{I}$  denotes the image from the camera obtained at  $t$ . The convolutional layers of ResNet50 [14] are utilized to extract visual context vectors  $\mathbf{V} = [\mathbf{v}_1, \dots, \mathbf{v}_M]$  from  $\mathbf{I}$ , where  $\mathbf{V}$  is the output of the last convolutional layer of ResNet50 and  $M$  denotes the spatial resolution of the output.

**PGN** In section 4.1, we defined a path as a series of position vectors. In this paper, it is assumed that, when determining a path that matches a driving intention, human drivers sequentially locate each position according to the corresponding intention determined by their past movements and scene context information. For example, to make a left turn, human drivers determine multiple paths a few meters away from the corner in the following order: 1) keep or decrease the speed (a series of *Go*), 2) make a left turn (a series of *Turn Left*), and 3) settle in a target lane (a series of *Go*). Based upon this assumption, we device an interaction model between the positions and intentions, and encourage PGN not only to generate positions in a path but also to capture the hidden intentions at the same time. The proposed interaction model encourages PGN to generate more accurate and diverse paths as seen in section 5.

Fig. 3-(a) briefly describes the structure of PGN. It consists of two LSTM networks, one for the path generation ( $LSTM_P$ ) and the other for the intention decision ( $LSTM_A$ ). Let  $a_l$  and  $\mathbf{a}_l \in \mathbf{R}^{|\mathcal{A}|}$  denote the hidden intention for  $\mathbf{p}_l$  and a vector representation of  $a_l$ , respectively.  $\mathbf{p}_l$  is determined with  $\mathbf{a}_l$  via  $LSTM_P$  as follows:

$$\mathbf{e}_{l-1}^p = \phi_{Relu}([\mathbf{p}_{l-1}; \mathbf{a}_l]), \quad (1)$$

$$\mathbf{h}_l^p = LSTM_P(\mathbf{e}_{l-1}^p, \mathbf{h}_{l-1}^p), \quad (2)$$

$$\mathbf{c}_l = ATT_P(\mathbf{h}_l^p, \mathbf{V}), \quad (3)$$

$$\mathbf{p}_l = \phi(\phi_{Relu}([\mathbf{c}_l; \mathbf{h}_l^p])), \quad (4)$$

where  $[\cdot; \cdot]$  and  $ATT_P$  denote the concatenation and spatial attention operation [20], respectively, and  $\phi$  and  $\phi_{Relu}$  respectively denote fully-connected layers with linear and

Relu activation functions. We initialize the hidden state of  $LSTM_P$  as

$$\mathbf{h}_0^p = \phi_{Relu}([\phi_{Relu}(\bar{\mathbf{a}}); \mathbf{n}]), \quad (5)$$

where  $\bar{\mathbf{a}}$  is an onehot vector representation of  $a$ ,  $\mathbf{n}$  is a random noise vector drawn from Gaussian distribution with mean 0 and standard deviation 1. In addition, we use the speed  $s$  for the initial position  $\mathbf{p}_0 = [s, s]^T$ .

The hidden intention  $a_l$  is determined as follows:

$$\mathbf{e}_{l-1}^a = \phi_{Relu}([\mathbf{a}_{l-1}; \mathbf{p}_{l-1}; \mathbf{h}_{l-1}^p; \mathbf{c}_{l-1}]), \quad (6)$$

$$\mathbf{h}_l^a = LSTM_A(\mathbf{e}_{l-1}^a, \mathbf{h}_{l-1}^a), \quad (7)$$

$$\mathbf{a}_l = \phi(\mathbf{h}_l^a). \quad (8)$$

We use a zero vector for the initial hidden state of  $LSTM_A$ ,  $\mathbf{h}_0^a$ , and use  $\bar{\mathbf{a}}$  for  $\mathbf{a}_0$ .

**DN** Fig. 3-(b) briefly describes the structure of DN. It consists of two LSTM networks, one for the path discrimination and classification ( $LSTM_{D_1}$ ) and the other for the discrimination of sequences of intentions ( $LSTM_{D_2}$ ). DN takes  $\mathbf{P}_a$  and  $\mathbf{V}$  as inputs and outputs  $d_{scr1} \in [0, 1]$  and  $\mathbf{c}_{cls} \in \mathbf{R}^{|\mathcal{A}|}$  as follows.

$$\mathbf{e}_{l-1}^{d_1} = \phi_{Relu}(\mathbf{p}_{l-1}), \quad (9)$$

$$\mathbf{h}_l^{d_1} = LSTM_{D_1}(\mathbf{e}_{l-1}^{d_1}, \mathbf{h}_{l-1}^{d_1}), \quad (10)$$

$$\mathbf{c}_l = ATT_D(\mathbf{h}_l^{d_1}, \mathbf{V}), \quad (11)$$

$$d_{scr1} = \phi_{sig}(\sum_{l=1}^L \mathbf{h}_l^{d_1}), \quad (12)$$

$$\mathbf{c}_{cls} = \phi(\sum_{l=1}^L \phi_{Relu}[\mathbf{h}_l^{d_1}; \mathbf{c}_l]), \quad (13)$$

where  $\phi_{sig}$  and  $ATT_D$  denote a fully-connected layer with sigmoid activation function and the spatial attention operation [20], respectively.

It also takes  $\mathbf{A} = \{\bar{\mathbf{a}}_l\}_{l=1}^L$  as an input and outputs  $d_{scr2} \in [0, 1]$  as follows.

$$\mathbf{e}_{l-1}^{d_2} = \phi_{Relu}(\bar{\mathbf{a}}_{l-1}), \quad (14)$$

$$\mathbf{h}_l^{d_2} = LSTM_{D_2}(\mathbf{e}_{l-1}^{d_2}, \mathbf{h}_{l-1}^{d_2}), \quad (15)$$

$$d_{scr2} = \phi_{sig}(\mathbf{h}_L^{d_2}), \quad (16)$$

where  $\bar{\mathbf{a}}_l$  is the onehot vector representation of  $a_l$ . Finally, note that we use zero vectors for the initial hidden states  $\mathbf{h}_0^{d_1}$  and  $\mathbf{h}_0^{d_2}$ .

$d_{scr1}$  indicates if the input path comes from the dataset or PGN. Equation 12 shows that  $d_{scr1}$  is determined by  $\{\mathbf{h}_l^d\}$ , which are calculated from the positions only. This implies that DN only considers the shape of the path for the path

discrimination. On the other hand,  $\mathbf{c}_{cls}$  indicates which category of driving intention the input path falls into. When calculating  $\mathbf{c}_{cls}$ , DN considers both the input path and visual contexts simultaneously through the attention mechanism as seen in Eqn. 13. Finally,  $d_{scr2}$  indicates if the sequence of the intentions for the path is real or fake. As a result, PGN guided by DN through the adversarial training will produce paths that are realistic and match the driving intentions.

### 4.3. Losses

**Variety loss** To encourage PGN to produce diverse paths, we use the variety loss [13, 29] defined as follows.

$$\mathcal{L}_{var} = \min_k \frac{1}{L} \|\mathbf{P}_a^{gt} - \mathbf{P}_a^k\|_2^2, \quad (17)$$

where  $\mathbf{P}_a^{gt}$  is the ground-truth path from the dataset.

**Adversarial losses** For simplicity purposes, let  $c$  denote the conditional inputs  $(\mathbf{I}, a, s)$ . We define two adversarial losses, one for a path  $\mathbf{P}$  and the other for a sequence of intentions  $\mathbf{A}$  as follows.

$$\begin{aligned} \mathcal{L}_{adv1} = & \mathbb{E}_{\mathbf{P} \sim p_{data}} [\log D_1(\mathbf{P})] \\ & + \mathbb{E}_{\mathbf{z} \sim p_z} [\log(1 - D_1(G_p(\mathbf{z}|c)))] \end{aligned} \quad (18)$$

$$\begin{aligned} \mathcal{L}_{adv2} = & \mathbb{E}_{\mathbf{A} \sim p_{data}} [\log D_2(\mathbf{A})] \\ & + \mathbb{E}_{\mathbf{z} \sim p_z} [\log(1 - D_2(G_a(\mathbf{z}|c)))] \end{aligned} \quad (19)$$

where  $D_1$  and  $D_2$  respectively denote the path and sequence discrimination networks. In addition,  $G_p$  and  $G_a$  denote the generation networks for the path and sequence, respectively.

**Classification losses** We define two classification losses, one for  $a$  and the other for  $\mathbf{A}$  as follows.

$$\mathcal{L}_{cls1} = BCE(\bar{\mathbf{a}}, \text{softmax}(\mathbf{c}_{cls})), \quad (20)$$

$$\mathcal{L}_{cls2} = \frac{1}{L-1} \sum_{l=2}^L BCE(\bar{\mathbf{a}}_l, \text{softmax}(\mathbf{a}_l)). \quad (21)$$

We use the ground-truth intentions given in our dataset for  $\bar{\mathbf{a}}$  and  $\bar{\mathbf{a}}_l$  (the onehot vector representations of  $a$  and  $a_l$ , respectively) for the calculation of the losses.

**Full objective** The final objective functions to be minimized are written as follows.

$$\mathcal{L}_G = \lambda_1 \mathcal{L}_{var} + \mathcal{L}_{adv1} + \mathcal{L}_{cls1} + \lambda_2 \mathcal{L}_{adv2} + \lambda_3 \mathcal{L}_{cls2}, \quad (22)$$

$$\mathcal{L}_D = -\mathcal{L}_{adv1} - \lambda_4 \mathcal{L}_{adv2} + \mathcal{L}_{cls1}. \quad (23)$$

## 5. Experiments

### 5.1. Evaluation Methodology

There are 131 sequences of length 10 minutes in *ETRIDriving*. For evaluation, we choose 32 (25 for training and 7 for test) out of the 131 sequences, which have diverse driving actions of the ego-vehicle, since, in most sequences, the vehicle went straight or kept stopping most of the time. The samples  $(\mathbf{I}, \mathbf{P}_a, a, \mathbf{A}, s)$  for training and test are generated from the 32 sequences as follows. First, a transformation matrix  $\mathbf{M}_t$  is created from the yaw, pitch, roll, and global position of the vehicle at current time index  $t$ . We use  $\mathbf{M}_t$  to represent the future trajectory of the vehicle in the egocentric coordinate system. Each position in  $\mathbf{P}_a$  is then obtained by using the positions in the transformed trajectory under the constraints  $\|\mathbf{p}_l - \mathbf{p}_{l+1}\|^2 = 1$ ,  $\mathbf{p}_0 = [0, 0]^T$ . We set  $L = 20$ , which means the length of a path is 20 meters. For  $a_l \in \mathbf{A}$ , we find the position in the trajectory nearest to  $\mathbf{p}_l$  and use the driving action label assigned to the position. For  $a$ , we choose one action from  $\{a_l\}_{l=1}^F$  where  $F \leq L$ . However, it is not easy to choose one action that matches the “true” driving intention of the ego-vehicle exactly when there are more than two actions in  $\{a_l\}_{l=1}^F$ . So we randomly pick an action from  $\{a_l\}_{l=1}^F$  during training so that the action constituting the majority of  $\{a_l\}_{l=1}^F$  is chosen for representing the driving intention of the path with a high probability. In contrast, during test, we choose the one constituting the majority of  $\{a_l\}_{l=1}^F$  for the consistency. Finally, the front-facing camera image and the speed of the ego-vehicle recorded at  $t$  are used for  $\mathbf{I}$  and  $s$ , respectively.

From the 32 sequences, we can obtain about 162,000 samples. However, we discard samples from trajectories obtained under low GPS accuracy. In addition, we discard some samples to balance the numbers of different actions in the dataset. As a result, 28,320 samples (21,876 for training and 6,444 for test) are finally used.

### 5.2. Baselines

The proposed model, which we call *PathGAN*, is compared with the following baselines:

- *CVAE*: Conditional variational autoencoder, which models generative distributions conditioned on sensory inputs and a driving intention. We follow a deep generative model proposed by Lee et al. [19] for the implementation.
- *CarNet*: Clairvoyant attentive recurrent network proposed by Sadeghian et al. [27]. We slightly modify the original implementation to make the network take a driving intention as an input.
- *E2ENet*: End-to-end model that generates a steering angle from a sensory input and a driving intention [8].
- *PathGen-single*: Single path generator (FEN and PGN) trained via MSE loss. We do not use  $a_l$  as an input to

$LSTM_P$ .

It is worth noting that, following the original implementations, we let *CVAE* and *CarNet* take as inputs the past trajectories of the ego-vehicle. In contrast, we design our model to use the current speed instead of the past trajectories since it is not easy to obtain the exact position and pose of the ego-vehicle consistently without HD maps.

### 5.3. Evaluation Metrics

We use five metrics to compare the methods objectively.

- Average Displacement Error (ADE): Average L2 distance between the ground truth and generated paths over all positions.
- Final Displacement Error (FDE): L2 distance between the last ground truth and generated positions.
- Diversity (Div): Average of ADE between paths generated from the same inputs.
- Marginal Log Likelihood (MLL): Average log-likelihood of the ground truth under the marginalized learned distribution for every positions [29].
- Mean Squared Error for Steering Angle (MSE-S): Squared error between the ground truth steering angle and the angle estimated from the generated path.

We introduce MSE-S to evaluate how suitable a generated path is to control the real vehicle. To produce a steering angle from a path, we train an LSTM network, which takes a path as well as a vehicle speed as inputs and outputs a steering angle, by using the ground-truth paths and steering angles. Note that we normalized the angles to be in range [-1, 1].

### 5.4. Implementation Details

The original input RGB image is first resized to have  $640 \times 320 \times 3$  pixels and then normalized to have pixel values in the range [-1, 1]. ResNet50 produces a feature map of size  $20 \times 10 \times 2048$  from the image. Therefore,  $\mathbf{v}_i$  is a vector of length 2048 and the number of elements in  $\mathbf{V}$  is 200. The dimension of the hidden state for  $LSTM_{D_2}$  is set to 32 while the dimensions of the others are set to 128. We iteratively train PGN and DN using Adam [18] with an initial learning rate of  $10^{-4}$  and a batch size 16 for 100 epochs. FEN is also trained simultaneously using the Adam with an initial learning rate of  $5 \times 10^{-5}$  after it is initialized by the trained parameters of FEN of *PathGen-single*.

### 5.5. Quantitative Evaluation

**Performance Comparison** We compare our model on the five metrics against the baselines and Table 1 shows the results. We can see in the table that our final model *PathGAN-4* outperforms the baselines in terms of the path generation accuracy (ADE, FDE, MLL) and the diversity (Div). As expected, *CarNet* and *PathGen-single* show performances worse than *PathGAN-4* since they can gener-

Method	Losses	ADE( $\downarrow$ )	FDE( $\downarrow$ )	Div( $\uparrow$ )	MLL( $\uparrow$ )	MSE-S( $\downarrow$ )
<i>E2ENet</i> [8]	-	-	-	-	-	$0.0055 \pm 0.0003$
<i>CarNet</i> [27]	-	$0.258 \pm 0.012$	$0.733 \pm 0.027$	-	-	$0.0029 \pm 0.0005$
<i>PathGen-single</i>	-	$0.339 \pm 0.002$	$0.868 \pm 0.022$	-	-	$0.0049 \pm 0.0005$
<i>CVAE</i> [19]	-	$0.164 \pm 0.012$	$0.402 \pm 0.003$	$1.405 \pm 0.599$	$-2.235 \pm 0.144$	$0.0125 \pm 0.0034$
<i>PathGAN-1</i>	$\mathcal{L}_{var}$	$0.284 \pm 0.018$	$0.694 \pm 0.04$	$0.258 \pm 0.019$	$-2.557 \pm 0.059$	$0.0064 \pm 0.0007$
<i>PathGAN-2</i>	$\mathcal{L}_{var}, \mathcal{L}_{adv1}, \mathcal{L}_{cls1}$	$0.144 \pm 0.004$	$0.366 \pm 0.017$	$0.340 \pm 0.004$	$-2.106 \pm 0.006$	$0.0036 \pm 0.0002$
<i>PathGAN-3</i>	$\mathcal{L}_{var}, \mathcal{L}_{adv1}, \mathcal{L}_{cls1}, \mathcal{L}_{cls2}$	$0.140 \pm 0.005$	$0.335 \pm 0.010$	$0.422 \pm 0.048$	$-2.098 \pm 0.011$	$0.0047 \pm 0.0009$
<i>PathGAN-4</i>	$\mathcal{L}_{var}, \mathcal{L}_{adv1}, \mathcal{L}_{adv2}, \mathcal{L}_{cls1}, \mathcal{L}_{cls2}$	$0.134 \pm 0.009$	$0.336 \pm 0.023$	$0.421 \pm 0.072$	$-2.101 \pm 0.003$	$0.0040 \pm 0.0004$

Table 1. Quantitative results of all methods when  $K = 20$ ,  $F = 5$ . ADE, FDE, and MSE-S are calculated by using the path with the minimum ADE among the  $K$  paths. To obtain the values in the table, we trained each model three times.

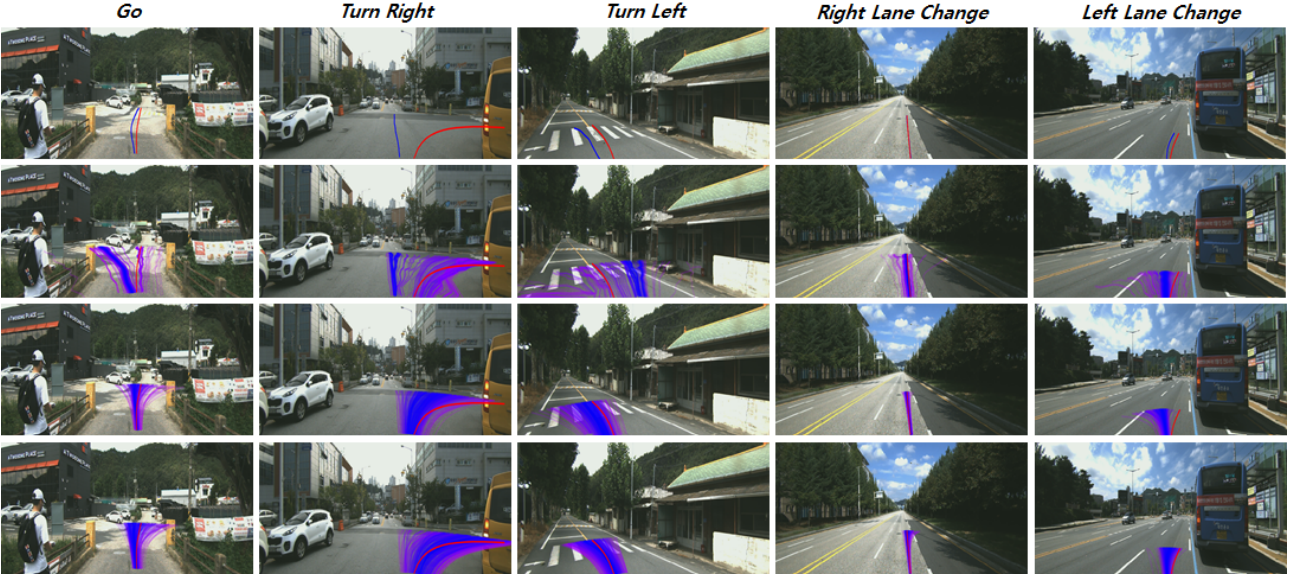


Figure 4. Path generation results. Each row is the results of *CarNet*, *CVAE*, *PathGAN-2*, and *PathGAN-4* in order. Red lines denote the ground-truth paths while blue and purple lines denote the generated paths. We use blue for highly probable paths and purple for less probable paths. Note that 300 paths are generated for each scene from the trained models listed in Table 1.



Figure 5. Path generation with various driving intentions. Each column is the results of *CarNet*, *CVAE*, and *PathGAN-4* in order. Red lines denote the ground-truth paths. Blue, green, yellow, and sky blue lines denote the paths generated with *Go*, *Turn Left*, *Turn Right*, and *U-Turn*, respectively.

ate only one path. *CVAE* shows performances better than *CarNet* and *PathGen-single* in terms of ADE and FDE as it can generate multiple paths. However, MLL and Div results of *CVAE* indicate that the paths generated by *CVAE* are

inaccurate even if the paths are diverse. On the other hand, *PathGAN-4* also shows a good performance on MSE-S. Particularly, it outperforms *E2ENet*, which estimates steering angles from I directly and has been successful in real-world driving [8, 3]. *CarNet* shows the best performance even if it generates a single path.

**Ablation Study** We do an ablation study of our model with four different settings as seen in Table 1: ***PathGAN-1***, FEN and PGN are trained to produce multiple paths via the variety loss (Eqn. 17) only; ***PathGAN-2***, the path discriminator and classifier are simultaneously trained under *PathGAN-1* setting; ***PathGAN-3***, PGN is encouraged to generate sequences of driving intentions under *PathGAN-2* setting; ***PathGAN-4***, the sequence discriminator is simultaneously trained under *PathGAN-3* setting. Note that we do not use  $\mathbf{a}_t$  as an input to  $LSTM_P$  for the implementations of ***PathGAN-1*** and ***PathGAN-2***. We can see in the table that introducing the path discriminator and classifier significantly improves the performance of PGN. In addi-

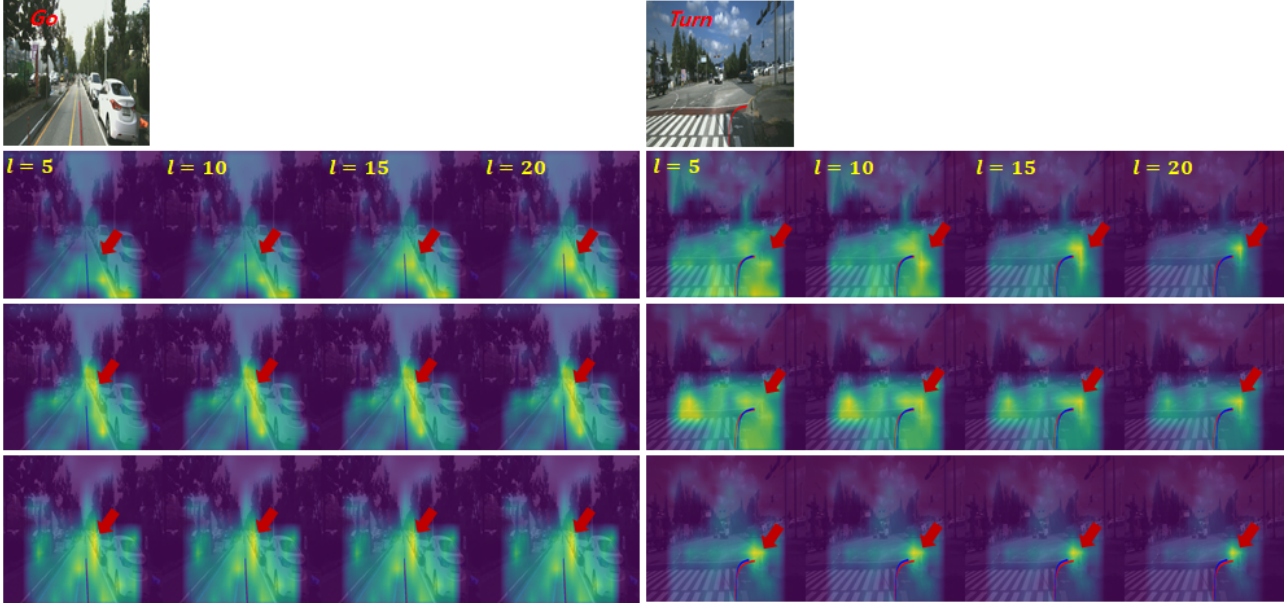


Figure 6. Visualization of attention regions for the generation of the fifth, tenth, fifteenth, and twentieth positions. The images in the first row are the input scenes. The second, third, and fourth rows are the results of *PathGAN-2*, *PathGAN-3*, and *PathGAN-4*, respectively.

tion, it is seen that the diversity of the generated paths is much improved while maintaining the accuracy by encouraging PGN to generate the sequences. This means that our model can generate multiple paths that are plausible and diverse. Finally, the generated paths become more suitable for real-world driving by the introduction of the sequence discriminator.

## 5.6. Qualitative Evaluation

We show in Fig. 4 the paths generated by each model. Each row in the figure is the results of *CarNet*, *CVAE*, *PathGAN-2*, and *PathGAN-4* in order. We can see in the figure that the paths from *PathGAN-4* are more accurate and diverse than those from the other models. Specifically, it is verified from the results of *PathGAN-2* and *PathGAN-4* that PGN can learn to generate accurate and diverse paths through the proposed interaction model described in section 4.2.

To test the ability to generate paths corresponding to different driving intentions from a driving scene, we let each model generate paths with various driving intentions from the scenes where more than one intention can be taken. Fig. 5 shows the results. Each column in the figure is the results of *CarNet*, *CVAE*, and *PathGAN-4* in order. It is seen in the figure that *PathGAN-4* successfully generates paths that are plausible and match the driving intentions. On the other hand, it seems that both *CarNet* and *CVAE* have trouble understanding the driving scenes so they fail to generate plausible paths match the intentions.

In Fig. 6, we show the image regions where PGN pays

attention to during the path generation process. The second, third, and fourth rows in the figure are the results of *PathGAN-2*, *PathGAN-3*, and *PathGAN-4*, respectively. We can see in the figure that *PathGAN-2* pays attention to different regions for each position. In contrast, both *PathGAN-3* and *PathGAN-4*, from the beginning of the generation process, pay attention to the regions required to generate all the positions, and then change their interests as the process progresses. On the other hand, it is also seen that *PathGAN-4* changes its interests more slowly than *PathGAN-3*.

## 6. Conclusion

In this paper, we proposed a generative model that can generate multiple plausible paths for the AV from an ego-centric view image given a driving intention and speed. To make the generated paths plausible and match the driving intention, we utilized the GANs framework where the path discrimination and classification networks are simultaneously trained with the generative model. The accuracy and diversity of the generated paths are further improved by incorporating the interaction model between positions in a path and intentions hidden in the positions. To evaluate the proposed model, we introduced *ETRIDriving*, the driving dataset labeled with the high-level driving actions, and verified the state-of-the-art performance of the model on *ETRIDriving* in terms of the accuracy and diversity.

## References

- [1] A. Alahi, K. Goel, V. Ramanathan, A. Robicquet, L. Fei-Fei, and S. Savarese. Social lstm: human tra-

jectory prediction in crowded spaces. In *IEEE International Conference on Computer Vision and Pattern Recognition*, pages 961–971, 2016. 2

[2] J. Aneja, H. Agrawal, D. Batra, and A. Schwing. Sequential latent spaces for modeling the intention during diverse image captioning. In *IEEE International Conference on Computer Vision*, October 2019. 2

[3] M. Bojarski, D. D. Testa, D. Dworakowski, B. Firner, B. Flepp, P. Goyal, L. D. Jackel, M. Monfort, U. Muller, J. Zhang, X. Zhang, J. Zhao, and K. Zieba. End-to-end learning for self-driving cars. In *arXiv:1604.07316*, 2016. 1, 2, 6

[4] P. Cai, Y. Sun, H. Wang, and M. Liu. Vtgnet: a vision-based trajectory generation network for autonomous vehicles in urban environments. In *arXiv:2004.12591*, 2020. 2

[5] S. Casas, W. Luo, and R. Urtasun. Intentnet: learning to predict intention from raw sensor data. In *Proceedings of The 2nd Conference on Robot Learning*, pages 947–956, 2018. 2

[6] C. Chen, A. Seff, A. Kornhauser, and J. Xiao. Deepdriving: Learning affordance for direct perception in autonomous driving. In *IEEE International Conference on Computer Vision*, pages 2722–2730, 2015. 1

[7] D. Choi, K. Min, and J. Choi. Regularizing neural networks for future trajectory prediction via inverse reinforcement learning framework. *IET Computer Vision*, 1(1):1–2, 2020. 2

[8] F. Codevilla, M. Miiller, A. Lopez, V. Koltun, and A. Dosovitskiy. End-to-end driving via conditional imitation learning. In *IEEE International Conference on Robotics and Automation*, pages 4693–4700, 2018. 1, 2, 5, 6

[9] M. Cordts, M. Omran, S. Ramos, T. Rehfeld, M. Enzweiler, R. Benenson, U. Franke, S. Roth, and B. Schiele. The cityscapes dataset for semantic urban scene understanding. In *arXiv:1604.01685*, 2016. 2

[10] L. Fang, Q. Jiang, J. Shi, and B. Zhou. Tpnet: trajectory proposal network for motion prediction. In *IEEE Conference on Computer Vision and Pattern Recognition*, pages 6709–6806, 2020. 2

[11] A. Geiger, P. Lenz, and R. Urtasun. Are we ready for autonomous driving? the kitti vision benchmark suite. In *IEEE Conference on Computer Vision and Pattern Recognition*, pages 3354–3361, 2012. 2

[12] L. Guo, J. Liu, P. Yao, J. Li, and H. Lu. Mscap: multi-style image captioning with unpaired stylized text. In *IEEE International Conference on Computer Vision and Pattern Recognition*, pages 4204–4213, 2019. 2

[13] A. Gupta, J. Johnson, L. Fei-Fei, S. Savarese, and A. Alahi. Social gan: socially acceptable trajectories with generative adversarial networks. In *IEEE International Conference on Computer Vision and Pattern Recognition*, pages 2255–2264, 2018. 2, 4

[14] K. He, X. Zhang, S. Ren, and J. Sun. Deep residual learning for image recognition. In *IEEE Conference on Computer Vision and Pattern Recognition*, pages 770–778, 2016. 3

[15] S. Hecker, D. Dai, , and L. V. Gool. End to end learning of driving models with surround-view cameras and route planners. In *European Conference on Computer Vision*, pages 450–464, 2018. 1, 2

[16] C. Katrakazas, M. Quddus, W. Chen, and L. Deka. Real-time motion planning methods for autonomous on-road driving: state-of-the-arts and future research directions. *Transportation Research Part C*, 60:416–442, 2015. 1

[17] J. Kim, T. Misu, Y.-T. Chen, A. Tawari, and J. Canny. Grounding human-to-vehicle advice for self-driving vehicles. In *IEEE Conference on Computer Vision and Pattern Recognition*, 2019. 2

[18] D. P. Kingma and L. J. Ba. Adam: a method for stochastic optimization. In *International Conference on Learning Representations*, 2015. 5

[19] N. Lee, W. Choi, P. Vernaza, C. B. Choy, P. H. S. Torr, and M. Chan. Desire: Distant future prediction in dynamic scenes with interacting agents. In *IEEE International Conference on Computer Vision and Pattern Recognition*, pages 2165–2174, 2017. 2, 5, 6

[20] J. Lu, C. Xiong, D. Parikh, and R. Socher. Knowing when to look: adaptive attention via a visual sentinel for image captioning. In *IEEE International Conference on Computer Vision and Pattern Recognition*, pages 375–383, 2017. 2, 3, 4

[21] W. Maddern, G. Pascoe, C. Linegar, and P. Newman. 1 Year, 1000km: the oxford RobotCar dataset. *The International Journal of Robotics Research*, 36(1):3–15, 2017. 2

[22] S. Malla, B. Dariush, and C. Choi. Titan: future forecast using action priors. In *IEEE Conference on Computer Vision and Pattern Recognition*, 2020. 2

[23] D. A. Pomerleau. Alvinn, an autonomous land vehicle in a neural network. In *Advances in Neural Information Processing Systems*, pages 305–313, 1988. 1

[24] N. Rhinehart, K. M. Kitani, and P. Vernaza. R2p2: a reparameterized pushforward policy for diverse, precise generative path forecasting. In *European Conference on Computer Vision*, pages 553–570, 2018. 2

[25] N. Rhinehart, R. McAllister, K. Kitani, and S. Levine. Precog: prediction conditioned on goals in visual multi-agent settings. In *IEEE International Conference on Computer Vision*, pages 2821–2830, 2019. 2

[26] A. Sadeghian, V. Kosaraju, A. Sadeghian, N. Hirose, H. Rezatofighi, and S. Savarese. Sophie: an attentive gan for predicting paths compliant to social and physical constraints. In *IEEE International Conference on Computer Vision and Pattern Recognition*, pages 1349–1358, 2019. [2](#)

[27] A. Sadeghian, F. Legros, M. Voisin, R. Vesel, A. Alahi, and S. Savarese. Car-net: clairvoyant attentive recurrent network. In *The European Conference on Computer Vision*, September 2018. [2](#), [5](#), [6](#)

[28] E. Santana and G. Hotz. Learning a driving simulator. In *arXiv:1608.01230v1*, 2016. [2](#)

[29] L. A. Thiede and P. P. Brahma. Analyzing the variety loss in the context of probabilistic trajectory prediction. In *IEEE International Conference on Computer Vision*, October 2019. [4](#), [5](#)

[30] Q. Wu, C. Shen, L. Liu, A. Dick, and A. v. d. Hengel. What value do explicit high level concepts have in vision to language problems? In *IEEE International Conference on Computer Vision and Pattern Recognition*, pages 203–212, 2016. [2](#)

[31] H. Xu, Y. Gao, F. Yu, , and T. Darrell. End-to-end learning of driving models from large-scale video datasets. In *IEEE International Conference on Computer Vision and Pattern Recognition*, pages 2774–2182, 2017. [1](#), [2](#)

[32] K. Xu, J. Ba, R. Kiros, K. Cho, A. Courville, R. Salakhudinov, R. Zemel, and Y. Bengio. Show, attend and tell: neural image caption generation with visual attention. In *International Conference on Machine Learning*, pages 2048–2057, 2015. [2](#)

[33] L. Yang and H. Hu. Visual skeleton and reparative attention for part-of-speech image captioning system. *Computer Vision and Image Understanding*, 189, 2019. [2](#)

[34] L. Yang, X. Liang, T. Wang, and E. Xing. Real-to-virtual domain unification for end-to-end autonomous driving. In *European Conference on Computer Vision*, pages 553–570, 2018. [1](#), [2](#)

[35] T. Yao, Y. Pan, Y. Li, Z. Qiu, and T. Mei. Boosting image captioning with attributes. In *IEEE International Conference on Computer Vision*, pages 4894–4902, 2017. [2](#)

[36] H. Yu, S. Yang, W. Gu, and S. Zhang. Baidu driving dataset and end-to-end reactive control model. In *IEEE Intelligent Vehicles Symposium*, pages 341–346, 2017. [1](#), [2](#)

[37] W. Zeng, W. Luo, S. Suo, A. Sadat, B. Yang, S. Casas, and R. Urtasun. End-to-end interpretable neural motion planner. In *IEEE International Conference on Computer Vision and Pattern Recognition*, pages 8660–8669, 2019. [2](#)